Coverage and Channel Characteristics of Millimeter Wave Band Using Ray Tracing

Zhenliang Zhang, Jung Ryu, Sundar Subramanian and Ashwin Sampath
Qualcomm CR&D
Bridgewater, New Jersey

***Abstract*—Utilization of millimeter wave (MMW) bands for supporting very high data rate cellular access has received much attention in recent times. The behavior of the wireless channel in these bands differ significantly from the sub-6 GHz counterparts. Ray tracing is a complementary effort to detailed measurements in providing quick insight into the coarse channel characteristics. In this paper, we model the 28 GHz outdoor channel through ray tracing using the WinProp tool. We simulate the single base station and multi base station scenarios in the downtown Manhattan area and study channel properties such as coverage and path loss, path diversity and delay spreads. We observe that a typical MMW base station provides coverage to a significant fraction of a 100m cell radius with path diversity, i.e. there exist secondary paths that may sustain the link on the failure of the first path. The improvements to coverage and path diversity with multiple base stations are also characterized. The above channel properties are compared with NYU's [4] results from the same region. We observe a reasonable match for many of the above parameters. The delay spreads with omni and beamformed antennas are also compared. The typical RMS delay spread in a beamformed scenario is seen to be in the order of 20-30 ns which is significantly smaller than the measured values of 100ns or more. This phenomenon is likely due to detailed clutter in the environment not being modeled.**

I. Introduction

There is a growing demand for data spurred by a variety of mobile applications ranging from always-on data for cloud services, high quality video conferencing to on-demand movies for mobile consumption. To satisfy the ever-increasing data demand, the next generation technology (5G) may support radically different techniques than current generations. Recent trends in RF technology have enabled the production of cost-effective radios capable of operating in carrier frequencies well above the traditional sub-6 GHz bands[11]. For example, the WiGig/802.11ad standard has been defined and products based on this standard are currently available, though mainly geared towards very short range applications (e.g. cable replacement, wireless docking etc.)[2]. The use of millimeter wave (MMW) frequencies ($>$ 10 GHz) to enable cellular data access is gaining attention and is being considered for next generation wireless technologies [14], [13].

Well-known approaches to increase the network throughput are (i) improving the spectral efficiency of a given link (better PHY layer techniques), (ii) using larger bandwidths and (iii) increasing the efficiency of spatial reuse (better MAC layer techniques). The use of millimeter wave bands allow significant gains along each of these dimensions. The capability of antennas to attain higher directivity at higher frequencies (for the same aperture size) enables the inherent beamforming to improve the signal strength and spectral efficiency. The frequency bands in the 28 GHz, 39 GHz and 60 GHz are currently lightly used and permit potentially large channel bandwidths. For instance, 28 GHz band has up to 1.3 GHz bandwidth, with the largest contiguous channel having a bandwidth of 850 MHz [1]. The 60 GHz band (which is currently unlicensed) has up to 7 GHz of available spectrum. The highly directive transmissions in millimeter bands naturally reduce interference and allow for very dense spatial reuse. In this paper, we study the behavior of the 28 GHz bands.

To ascertain the feasibility of millimeter wave band cellular access, (MM-Wave Access) characterization of the MMW channel is necessary. There are significant differences in the propagation of electromagnetic waves at MMW bands as compared to sub-6GHz bands. There are several complementary approaches to understanding the MMW channel; conducting well-planned and detailed measurement campaigns is an extremely valuable but expensive and time-consuming method. Extensive campaigns carried out recently by NYU [14] still only map about 20 receive locations and 3 transmit locations in one area of New York City. A quick alternative is to use ray-tracing methods to derive gross statistics about the channel. Such approaches have been successfully applied for lower frequencies [6].

In our paper, we describe our results of channel and capacity characterization obtained through ray tracing for the 28 GHz MMW band. To our knowledge, these are some of the first results describing various channel properties such as angular diversity, statistics on reflected and diffracted rays, coverage ranges for a highly urban outdoor environment. We contrast our results with the available 28 GHz measurements and other ray tracing results and highlight the main characteristics.

A. Main Contributions

We study the 28GHz wireless channel of an urban environment using the WinProp ray tracing simulation software. We use a 3D model of the building layout of downtown Manhattan and model the buildings as cuboidal structures with fixed electrical properties. The electrical properties were obtained through our sample material measurements. The WinProp modeling tool uses a Fresnel equation based approach for modeling reflections and diffractions. We consider both a single base station and a multi base station scenario and observe the following characteristics based on our ray tracing:

1) The coverage range for a single base station is roughly around 100m for a typical link budget, with the covered area having more than a few strong

978-1-4673-6432-4/15/$31.00 ©2015 IEEE

channel taps. However, fitting a path loss slope is quite difficult due to the wide variation in received power at similar distances. This observation matches well with reported measurement results. This indicates that the typical model of path loss exponent with additive lognormal shadowing may be insufficient in describing the fairly geometric channel. In the multi-cell case with an inter-site spacing of 200m, we observe that the probability of outage is significantly reduced (<7%). The diffraction does not appear to play a major role in coverage and most of the strong taps are either Line-of-sight (LoS) or reflected.

2) The regions having good signal strength also show diversity in the number and direction of channel taps. With beamforming, it is crucial to have a diversity path (either to same cell or to another cell) in case the current path gets obstructed. In our simulations, median number of rays above an SNR threshold of 0 dB is about 3, and has significant angular difference between the rays. The fraction of power between the strong tap and diversity tap is also studied, with second tap from the same base station about 7 dB weaker on average. In the multi-cell case, both the number of diversity paths and their power split is improved for inter-site spacings of 200m or lesser.

3) The RMS delay spread is characterized for the links with an omni antenna and a beamformed antenna. Our simulations show an omni RMS delay spread of the order of 60-100ns and a beamformed delay spread of the order of 20ns. These values are somewhat smaller than the measurement results reported by NYU (50ns average in beamformed) [14], and Samsung (30ns) [8]. We believe that the discrepancy is possible due to WinProp (and ray tracing in general) being unsuited to modeling detailed small objects and finer structure in the environment. While such small objects are invisible in lower bands, at higher frequencies, they reflect significant amounts of energy.

While ray tracing does not model small objects, foliage and other small scale phenomena, it is seen that the technique is useful in providing first order estimates on coverage, spatial distribution of clusters and the benefits of macrodiversity.

II. Related Work

There are several complementary approaches to understanding the MMW channel; conducting well-planned and detailed measurement campaigns is an extremely valuable method. Many research teams and universities have performed channel sounding and channel characterization for various millimeter wave bands. In [5], authors have detailed the measurement campaign in 28 GHz bands and the results obtained. The derived channel parameters were described in [4]. A summary of these measurements can be found in [14]. A few other research teams in Samsung [7] and Ericsson have also reported some preliminary measurement results. However, conducting measurement campaigns in every type of use-case (typical city blocks, shopping districts and mall areas, suburban houses, highways, etc., and many types of indoor environments) is time-consuming and expensive. An alternate approach for understanding the wireless channel is through ray tracing. The method captures the geometry of the environments and is especially useful in understanding the MMW channel which is expected to be quite specular. While ray tracing may not be able to model all the finer details of the environment, it can provide a very good characterization of gross channel statistics. A few recent papers have also described ray tracing results for MMW bands. In [7], ray tracing results for outdoor environments (using the building data for Ottawa) were provided, and in [10], [12], ray tracing results for indoor 60 GHz propagation were studied. In [9], ray tracing was performed for a 72 GHz channel and results reported. In our paper, we characterize the channel characteristics such as path loss, delay spread, path diversity for a single base station and extend these notions to typical multi-cell deployments.

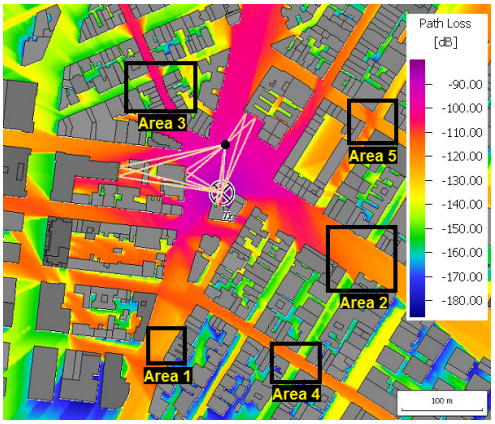

Fig. 1. The figure shows the path loss in the area around the transmitter located at 'X'. The white lines are the reflected/diffracted/scattered rays from the transmitter to the receiver (marked with a black dot) with path loss at most 125dB. The areas marked in black rectangles correspond to locations where the receive power measurements in Figure 2 are made.

III. Coverage and Path Loss Results

In this section, we present our simulation results on coverage and path loss. We break our presentation into two parts, first the single base station case, then the multi-base station case. In both cases, mmWave base stations are placed at a height of 10 meters above ground in downtown Manhattan near NYU campus. In our simulations, we model all of the buildings in the map as solid blocks with electrical properties of $\epsilon_r = 4$, $\mu_r = 1$, and $\sigma = 0.01$S/m; these electrical prosperities correspond to concrete commonly found in buildings. The signals can not penetrate buildings in our simulations. We only model buildings in our simulation environment; humans, cars, foilage, and other objects that are found in reality are not modeled. In addition, we do not model ground reflection. Details of how WinProp simulates reflections, diffractions, and scattering can be found in [3]. The locations we chose for the base station are at street intersections. We use the link budget in Table I to support 200Mbps or higher in the 500MHz bandwidth at 28GHz, which corresponds to the maximum path loss of 143dB or -5dB SNR.

Operating Frequency (GHz)	28
Transmitter Parameters	
Total Tx Power (dBm)	25
Number of Antennas	32 (16 × 2 planar array)
Array Gain (dB)	15.05
Per Elem. Antenna Gain (dB)	15
Total Antenna Array Inefficiency Loss (dB)	3
Net Transmit Antenna Array Gain (dB)	27.05
Total EIRP (dBm)	52.05
dBm per Element	9.95
Receiver Parameters	
Total Operating Bandwidth (MHz)	500
Noise Figure (dB)	11
Thermal Noise Power (dBm)	-87
Receive Antenna Gain (dB)	15
Rx Digital Inefficiency (dB)	5
Target Operating SNR (dB)	-5
Target Effective Data Rate (Mbps)	198.20
Maximum Supportable Pathloss(dB)	143.05

TABLE I. LINK BUDGET PARAMETERS - THE MAXIMUM PATH LOSS IS 143.05 DB IN ORDER TO SUPPORT 200MBPS OR HIGHER.

Interaction Modes	
Within 100m from base station	
LOS	57.5%
Reflection	22.2%
Diffraction	14.5%
Outage	5.8%
Within 200m from base station	
LOS	24.4%
Reflection	14.9%
Diffraction	38.7%
Outage	22%
Within 300m from base station	
LOS	14%
Reflection	9%
Diffraction	35.8%
Outage	41.2%

TABLE II. THE TABLE ABOVE SHOWS THE PERCENTAGE OF THE AREA WITHIN A FIXED DISTANCE FROM THE BASE STATION WITH THE DOMINANT BEAM CONTAINING ONE OF THE LISTED INTERACTION MODES.

A. Single Base Station

We performed three single base station simulation studies with the base stations placed at three different (but qualitatively similar, i.e., street intersections) locations. The path loss result from one of the locations we chose (Location 1) is shown in Figure 1. The mmW base station transmitter is at the location marked with an 'X'. The signal attenuates quickly as the Tx-Rx distance increases beyond 100-200m. In Figure 2, we plot the path loss at several locations near the mmW base station transmitter (Location 1). The figure shows that the path loss for a given Tx-Rx distance can vary widely, depending on actual location of the receiver and the geometry of the channel environment. The areas marked in black rectangles in Figure 1 correspond to locations where the receive SNR measurements in Figure 2 are made. Similar to our result shown here, the ray tracing simulation results from Samsung [7] show that the path loss can vary significantly between two different receiver locations that are at the same distance away from the transmitter. Since the propagation range for mmWave is relatively small, there can be wide variations in the number and types of propagation interactions two signals can experience even if the path lengths the two signals travel are the same. Hence, modeling propagation by a coarse path loss as a sole function of Tx-Rx separation distance will not give an accurate prediction of receive power. Contrast the path loss map at 28GHz in Figure 1 with that at 2.9GHz in Figure 3; the path loss over Tx-Rx separation distance in Figure 3 is over much narrower range than that of the same in Figure 1 (see Figure 2).

In Table II, we show the percentage of the outdoor area within a fixed distance from the base station with the dominant beam containing one of the listed interaction modes. For example, within a 100m radius circle from the base station, 57.5% of that area relies on LOS for the most dominant beam. In 22.2% of the area, reflected beams were the most dominant and had no LOS beams, and in 14.5% of the area, diffracted beams were the most dominant. (If a beam had combination of reflections and diffraction, we count that beam as a diffracted beam.) In 5.8% of the area, there was no detectable beam (i.e., no beam above -5dB SNR).

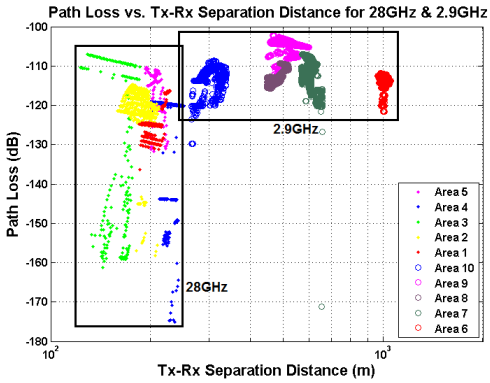

Fig. 2. The figure shows the path loss at the colored locations vs. the distance of the color locations from the transmitter (Location 1) at both 28GHz (Areas 1-5) and at 2.9GHz (Areas 6-10).

B. Multiple Base Stations

The base stations are manually placed on the NYC map with three different inter-site distances: 100, 200, and 300 meters. To eliminate edge effect (UEs on the edge have poor coverage and less interferences), we have also added more layers of base station beyond the base-stations with active UEs. At any given receiver/UE location, the UE establishes a link with the best base station/transmitter based on the beam formed SNR criteria.

The SNR/SINR plots are shown in Figure 4. The solid lines and dashed lines represent cumulative density plots for SNR and SINR, respectively. Notice that as the base station placement becomes denser, the SNR distribution becomes better due to base station diversity; and the outage probability becomes smaller. However, even with 100m inter-site distance, the outage tail still exists. It turns out most of the tail regime corresponds to UE locations that require steep diffraction angle (i.e., deep into the diffraction shadow region) to reach, which indicates that diffraction is not a dominant propagation mode at 28GHz frequency. For example, in the case of 200m inter-site distance, the strongest beam for 95% of the UEs with SNR $\leq$ 0dB comes from diffraction, while the strongest beam for over 98% of the UEs with SNR $>$ 0dB comes from line-of-sight or reflection. In addition, the base stations and UEs

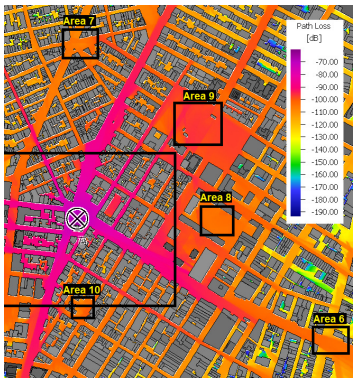

Fig. 3. The figure shows the path loss for 2.9GHz signal in the area around the base station (at height of 10m) located at 'X'. The map is approximately 1.4Km $\times$ 1.4Km. The figure shows that at 2.9GHz, the path loss (due to the geometry of the buildings) is very stable over distance, in contrast to what we see in Figure 1. The region in the black rectangle around the transmitter is that shown in Figure 1.

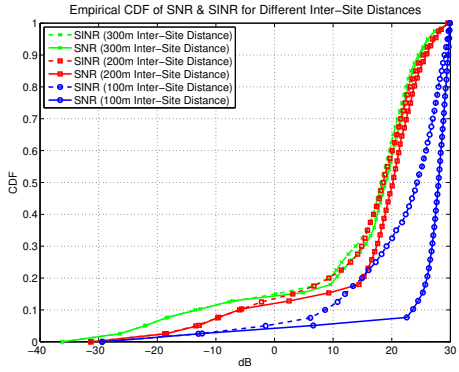

Fig. 4. CDF plots for SNR/SINR for different inter-site distance.

do not coordinate their beam forming directions, and hence interference can be further reduced for denser base station placement with 200m inter-site distance by using beamforming coordination between neighboring base stations. In Figure 4, a max SNR of 30dB is assumed and the realized SNR is the harmonic mean of SNR from WinProp and max SNR.

IV. Beam Diversity

A. Single Base Station

While path loss describes the overall strength of the rays that are possible from the base station to a receive location, the statistics on the number of beams that arrive at a receiver that exceeds certain power threshold is an important quantity. In the case when the dominant direction fails (due to small-scale fading, obstructions by objects), the presence of an alternate path from a different angle is necessary to maintain connectivity. The statistics of the diversity paths (for the single and multi-cell case) are presented in this section.

First, we situate one base station (at 3 possible locations), and plot the CDF of the number of receive beams/clusters exceeding a detectability threshold at all receive locations in the map where at least one beam of receive SNR of -5dB

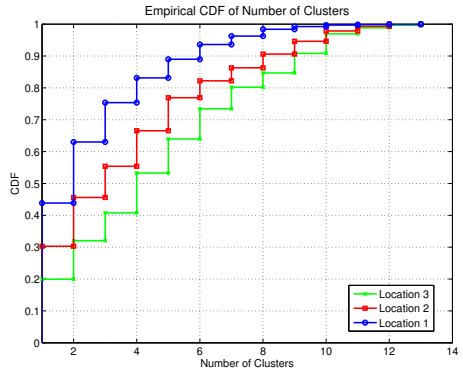

Fig. 5. The figure shows the CDF of the number of clusters (beams) with receive SNR of ≥ -5dB. Received rays that are too close (i.e., their angular separation is less than 10°) are counted as one cluster. The measurement results from [4] show that the receiver detects on median there are two or more beams.

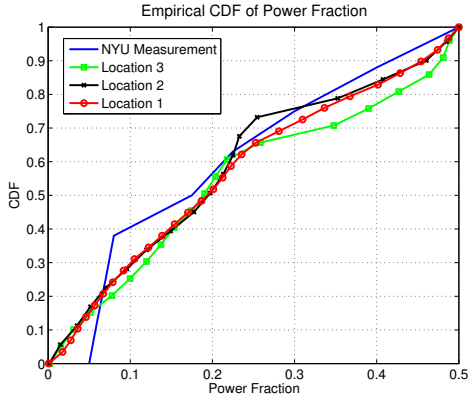

Fig. 6. The figure shows the CDF of the power fraction of the second strongest beam. Our simulation result shows that on median, the second strongest beam is about 7 dB weaker than the strongest beam. The second strongest beam is at least 10° away from the strongest beam, both in azimuth and elevation. Both the strongest and the second strongest beams must have receive SNR of $\geq$ -5dB. Our simulation result here similar to the findings reported in [4].

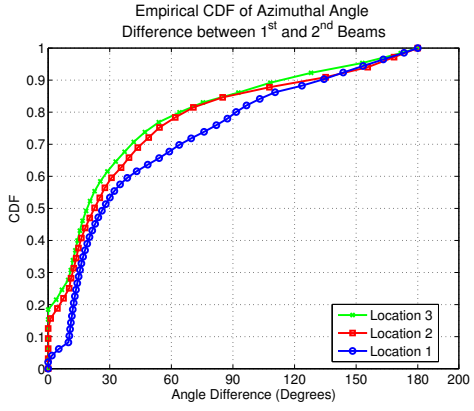

Fig. 7. The figure shows the CDF of the difference in the azimuthal angle of arrival of the strongest beam and the second strongest beam. The second strongest beam is at least 10° away from the strongest beam, either in azimuth or elevation or both. Both the strongest and the second strongest beams must have receive SNR of $\geq$ -5dB.

or greater can be detected (Figure 5). Each line in Figure 5 represents one of the three different locations base station locations we simulated. We see that on average there are about 2 to 4 detectable beams, even with a single mmW base station.

In Figure 6, we plot the CDF of the power fraction of the second dominant beam to the most dominant beam. We define the power fraction as

$$\frac{\text{RX power of } 2^{\text{nd}}\text{strongest beam}}{\text{Sum RX power of } 1^{\text{st}} \text{ and } 2^{\text{nd}} \text{ strongest beams}}.$$

Both the most dominant and the second dominant beams exceed a detectability threshold, i.e. the receive power of the two beams are at least -5dB SNR. On median, the simulation results show that the second dominant beam is about 6.5dB weaker than the most dominant beam. In Figure 7, we plot the azimuthal angular difference between the most dominant receive beam and the second most dominant receive beam, both exceeding a detectability threshold, i.e. the receive SNR of the two beams are at least -5dB SNR. The results show that in about 50% of the cases, the two beams are separated by about 25° or more in azimuth.

The measurement data from NYU [4] shows similarity with our results. NYU measurements show that on median the second strongest beam is 7dB weaker than the strongest beam (compare to Figure 6). NYU data also shows that with probability more than 0.5, two clusters will be detected; this result is similar to what we observe in our simulation result in Figure 5. Their data on AoA RMS angular spread (azimuthal) shows that on median, the spread is about 10°, and our result shows that on median, AoA azimuthal separation between the strongest and the second strongest beams is about 20° on median.

B. Multi Base Station

Next, we study the number of viable alternate paths at various base stations densities. In comparison to Figure 8, we plot the number of paths above the -5 dB threshold over all the receive locations. We observe in Figure 8, that the number of alternate paths increases steadily with decreasing inter-site distances. In fact, ray tracing suggests that there are more than 40 beams (median) at an inter-site spacing of 100m, underlining the extent of macro-diversity available.

The fraction of power split between the best path and the second best path is an indicator of the utility of the second best path to maintain coverage in the event the primary path is blocked or obstructed. In Figure 9, we notice that in the intra-cell case, the second path from the same cell is about 8 dB weaker, with the second path getting weaker with larger inter-site distance. When we consider secondary paths from any cell, the power fraction is significantly improved, with the second tap only being about 5 dB weaker. When compared to the single base station scenario, it appears that the power fraction is lower in the multi-cell scenario, but this is mainly due to the presence of strong LoS tap being more likely with higher densities. Further, the AoA of the strongest tap and the second strongest tap has about 20° separation on the average (see Figure 10).

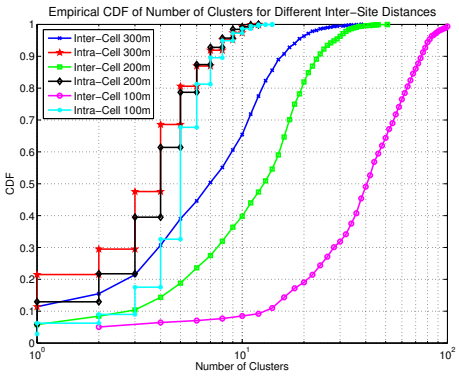

Fig. 8. Number of clusters observed above -5dB SNR from the best base station and all base stations for different inter-site distances.

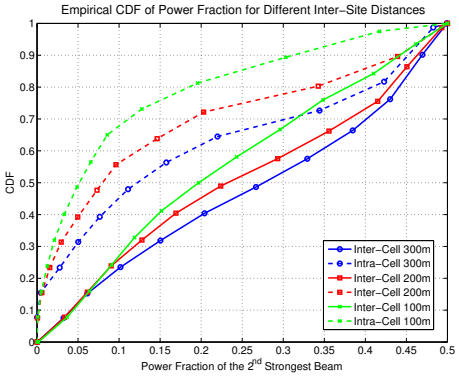

Fig. 9. The fraction of second largest beam (inter-cell and intra-cell) for different inter-site distances. For example, with inter-site distance 100m, the red solid line plots the CDF of the fraction of power of the second largest beam among the sum of the first two largest rays from the best base station.

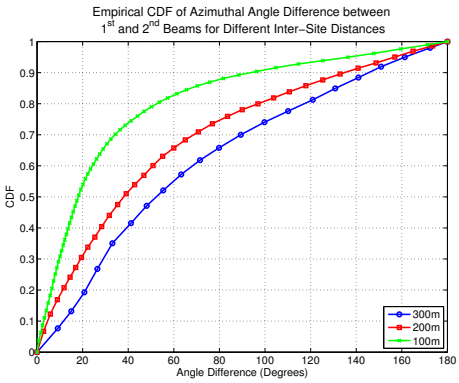

Fig. 10. The difference of AOA between the largest beam and the second largest beam for different inter-site distances.

V. Delay Spread

The simulation results in Figure 11 describe the delay spread with an omni antenna and a beamformed antenna. In our ray tracing results, we observe that the distribution of the beamformed delay spread is of the order of 20-40ns. There are rare cases where the delay spreads are above 100ns with

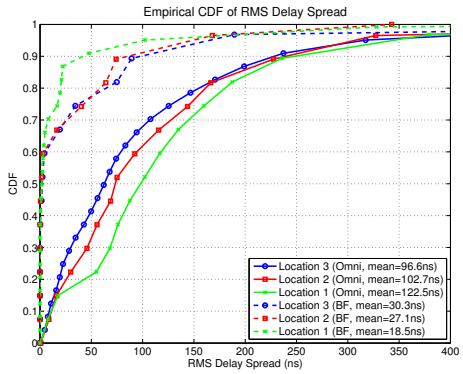

Fig. 11. The figure shows the CDF of the beam formed RMS delay. The beam formed RMS delay is obtained by having the receiver pointing its RX beam in the direction of the strongest incoming beam.

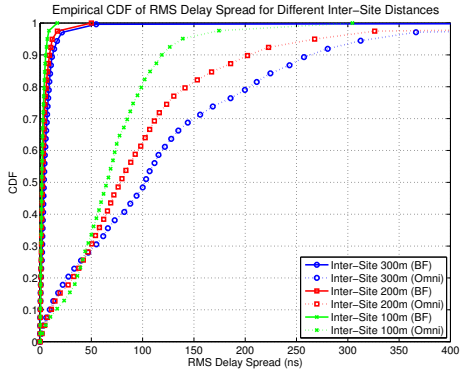

Fig. 12. The RMS delay spread for different inter-site distances.

beamforming. The omni delay spreads are of the order of 60-100ns.

Figure 12 describes the delay spread observed by a receiver from its best serving cell in a multi-cell scenario. We see that the same trend is extended - the omni RMS delay spreads are around 100ns while the beamformed delay spreads are much lesser (10-20ns) at all inter-cell spacings.

The simulation results from Samsung [8] report that the omni-directional RMS delay spread is on average about 35ns. On the other hand, the outdoor measurement results from NYU [4] show numerous instances of large RMS delay spread even with beamforming ($\sim$400ns). The NYU measurement results show larger delay spread because their channel measurement environment (downtown Manhattan) contains many small objects that produce many channel taps, whereas our WinProp simulations contain no such small objects; small objects such as light poles, cars, and metallic trash cans become more reflective as the carrier frequency increases. The comparisons with measured results indicate that ray tracing approaches may inherently underestimate the delay spreads.

VI. Conclusions

In conclusion, we note that ray tracing approaches are useful to model gross properties of the MMW channel. Our ray tracing results for a highly urban outdoor environment at 28 GHz match the path loss measurements and cluster diversity measurements from literature. The large spreads in path loss at similar distances indicate that a path loss model based on an attenuation exponent with an additive lognormal shadowing may be insufficient. The multi-cell simulations show that 200m or lesser inter-cell spacings are likely required to provide robust coverage in the MMW bands. The delay spread estimates from ray tracing in general are lesser than measured values, potentially from the inability of ray tracers to model smaller objects and their contributions to additional rays.

References

[1] FCC. http://wireless.fcc.gov/auctions/data/bandplans/lmds.pdf.

[2] Wilocity. http://wilocity.com/products/chipsets.

[3] WinProp User Manual. http://www.awe-communications.com.

[4] M. R. Akdeniz, Y. Liu, S. Sun, S. Rangan, T. S. Rappaport, and E. Erkip. Millimeter wave channel modeling and cellular capacity evaluation. *arXiv preprint arXiv:1312.4921*, 2013.

[5] Y. Azar, G. N. Wong, K. Wang, R. Mayzus, J. K. Schulz, H. Zhao, F. Gutierrez, D. Hwang, and T. S. Rappaport. 28 ghz propagation measurements for outdoor cellular communications using steerable beam antennas in new york city. In *Communications (ICC), 2013 IEEE International Conference on*, pages 5143–5147. IEEE, 2013.

[6] G. German, Q. Spencer, L. Swindlehurst, and R. Valenzuela. Wireless indoor channel modeling: statistical agreement of ray tracing simulations and channel sounding measurements. In *Acoustics, Speech, and Signal Processing, 2001. Proceedings.(ICASSP'01). 2001 IEEE International Conference on*, volume 4, pages 2501–2504. IEEE, 2001.

[7] S. Hur, Y. C, S. Baek, Y. Lee, and J. Park. mmwave propagation models based on 3d ray-tracing in urban environments. 2014. www.ic1004.org/uploads/Abstracts/Aalborg/TD(14)10054.pdf.

[8] S. Hur, Y.-J. Cho, K. Lee, J.-H. Ko, and J. Park. Millimeter-wave Channel Modeling based on Measurements in In-building and Campus Environments at 28 GHz. 2014. www.ic1004.org/uploads/Abstracts/Aalborg/TD(14)10053.pdf.

[9] S. G. Larew, T. A. Thomas, M. Cudak, and A. Ghosh. Air interface design and ray tracing study for 5g millimeter wave communications. In *Globecom Workshops (GC Wkshps), 2013 IEEE*, pages 117–122. IEEE, 2013.

[10] B. Neekzad, K. Sayrafian-Pour, J. Perez, and J. Baras. Comparison of ray tracing simulations and millimeter wave channel sounding measurements. In *Personal, Indoor and Mobile Radio Communications, 2007. PIMRC 2007. IEEE 18th International Symposium on*, pages 1–5, Sept 2007.

[11] A. M. Niknejad and H. Hashemi. *mm-Wave Silicon Technology*. Springer, 2008.

[12] W. Peter, W. Keusgen, and R. Felbecker. Measurement and ray-tracing simulation of the 60 ghz indoor broadband channel: Model accuracy and parameterization. In *Antennas and Propagation, 2007. EuCAP 2007. The Second European Conference on*, pages 1–8, Nov 2007.

[13] Z. Pi and F. Khan. An introduction to millimeter-wave mobile broadband systems. *Communications Magazine, IEEE*, 49(6):101–107, 2011.

[14] T. S. Rappaport, S. Sun, R. Mayzus, H. Zhao, Y. Azar, K. Wang, G. N. Wong, J. K. Schulz, M. Samimi, and F. Gutierrez. Millimeter wave mobile communications for 5G cellular: It will work! *Access, IEEE*, 1:335–349, 2013.